Advanced Series in Physical Chemistry 16

OVERVIEWS OF RECENT RESEARCH ON ENERGETIC MATERIALS

Editors

Robert W Shaw
Army Research Office, USA

Thomas B Brill
University of Delaware, USA

Donald L Thompson
University of Missouri, USA

World Scientific

Published by

World Scientific Publishing Co. Pte. Ltd.
5 Toh Tuck Link, Singapore 596224
USA office: 27 Warren Street, Suite 401-402, Hackensack, NJ 07601
UK office: 57 Shelton Street, Covent Garden, London WC2H 9HE

British Library Cataloguing-in-Publication Data
A catalogue record for this book is available from the British Library.

OVERVIEWS OF RECENT RESEARCH ON ENERGETIC MATERIALS

ISBN 981-256-171-4

Typeset by Stallion Press
Email: enquiries@stallionpress.com

"... Which, into hollow engines, long and round,
Thick rammed, at the other bore with touch of fire
Dilated and infuriate, shall send forth
From far, with thundering noise, among our foes
Such implements of mischief, as shall dash
To pieces, and o'erwhelm whatever stands
Adverse ..."

Paradise Lost

CHAPTER 3

STUDY OF ENERGETIC MATERIAL COMBUSTION CHEMISTRY BY PROBING MASS SPECTROMETRY AND MODELING OF FLAMES

Oleg P. Korobeinichev

Institute of Chemical Kinetics and Combustion
Siberian Branch Russian Academy of Sciences
630090 Novosibirsk, Russia

Contents

1. Introduction

Progress in the understanding of energetic material (EM) combustion will arise from a clearer picture of the chemistry and physics that take place in flames. We now recognize that the combustion of EMs is a complex multi-stage process based on the chemical transformations in the condensed and gas phases. Much more detailed information about the combustion chemistry of EMs is required. It is important to understand the combustion chemistry because this is the type of information a propellant formulator or a chemist

may use to tailor and/or improve the performance of the propellant.[1] The theories of Zel'dovich[2] and others on combustion of gun powder and explosives have played an important role in the development of the combustion theory of EMs. But, due to their simplified assumptions about the EM combustion mechanism and kinetics of reactions, they could not obtain satisfactory agreement with experiments on burning rates and their dependence on pressure and initial temperatures. New developments in advanced numerical methods and experimental techniques have enabled progress in the understanding of EM combustion chemistry, kinetics and mechanisms of chemical reactions in flames, and the derived combustion models much better describe the characteristics of burning EMs and the structures of their flames.

Studies of EM combustion have mostly investigated physical characteristics and neglected chemistry because of the experimental difficulties of studying chemical reactions in EM combustion waves. These difficulties are due to the high reaction rates (reaction times in condensed phases are of the order 10^{-1}–10^{-5} s), the high temperatures (up to 3000 K in the flame zone), the narrow spatial zones (of the order of 10^{-3} mm in the condensed phase and 10^{-1}–1 mm in the gas phase), the high burning rates, and the short time available for experiment (0.1–10 s). The difficulties are increased by the presence of heterogeneity and multiple ingredients. Although studies of combustion have been intensively conducted for about 60 years, only during the last decade has appreciable progress been achieved.

Our knowledge of the combustion chemistry of EMs comes mostly from flame structure studies.[3] These studies allow us to identify species in flames and to measure temperature and species concentration and their spatial distributions.[3–16] Analysis of the data on EM flame structures provides information on the composition of the condensed phase reaction products that are produced by EM thermal decomposition on the burning surface. These analyses, in turn, enable understanding of reactions in the condensed phase and their mechanisms. On the other hand, the chemical structure of the EM flame also provides information on the mechanisms and kinetics of gas-phase chemical reactions of further transformations of products emerging from the surface. These reactions are responsible for heat release in flames.

The principal methods applied to the investigation of chemical and thermal flame structures of EMs are: (1) probing mass-spectrometry (PMS),[4–9] (2) spectroscopic methods[1,10–16] for absorption and emission, including planar laser induced fluorescence (PLIF), spontaneous Raman scattering (SRS), coherent anti-Stokes Raman spectroscopy (CARS), and (3) the micro thermocouple technique.[17] Systematic studies of EM flame structures

using laser spectroscopic methods have been done mainly by Parr and Hanson-Parr[11,13,14,16] and Vanderhoff *et al.*[10,15] Spectroscopic methods are relatively non-intrusive; but there are many species in flames (very often the key species) which cannot be detected spectroscopically (see the chapter by Dagdigian). For example, the spectra of important species may be inaccessible because of wavelength or apparatus sensitivity limits.

Until recently there were few studies of EM flame structure. The improvement of experimental techniques, however, along with the development of flame-structure modeling and the rise of interest in EM combustion chemistry, has significantly increased the number of studies and their results have been used to understand EM combustion chemistry, to create chemical kinetics mechanisms of reactions in EM flames, and to develop EM combustion models.

This paper describes briefly the PMS method for EM flame structure studies and presents the results of the application of this method to EMs such as AP, RDX, HMX, ADN and some composite solid propellants (SP).

2. Experimental Techniques

Probing mass spectrometry (PMS) is one of the most effective and universally used experimental techniques for studying EM flame structures. Heller and Gordon[18] performed some of the first studies using a capillary probe to sample a double-base propellant flame at 10–20 atm. The closest approach of the probe to the burning surface was 1 mm; the surface was held at a constant position using a gold wire or quartz fiber restraint upon the propellant strand, which was pushed from below by a compressed spring. We developed an improved method[19–21] allowing the detection *in situ* of many species in the flame and the determination of their concentrations and their spatial distributions. In this improved method, a burning strand of EM moves with a velocity exceeding the burning rate toward a probe so that the probe continuously samples gaseous species from all the zones including those next to the burning surface. The probe ensures free gas-dynamic expansion of the sample accompanied by a rapid decrease in temperature and pressure and, hence, freezing of the mixture composition, which allows detection of atoms and free radicals. A skimmer placed after the probe cuts out the central part of a supersonic jet: free from possible heterogeneous and catalytic reactions on internal hot walls of the probe. The sample is then transported to the ion source of a time-of-flight (TOF) or quadruple mass spectrometer (again, the beam is not permitted to collide with the apparatus). Mass

spectra of samples are recorded with simultaneous filming of the probe and the burning surface. We have described the electronic system for stabilization of the EM burning surface using microthermocouples.[20]

2.1. *Microprobe and Molecular Beam Mass Spectrometric Techniques*

Two types of apparatus have been developed to study flame structure. The sample is transported to an ion source (1) as a molecular flow using a microprobe (MPT) with an inlet orifice of 10–20 micron, or (2) as a molecular beam (MBT) using a sonic probe with an inlet orifice of 20–200 micron. The microprobe has high spatial resolution and only slightly disturbs the flame, allowing the study of flames with a narrow combustion zone of 0.1 mm or less. Radicals, however, may recombine and unstable species, including EM vapors, may decompose and react on the inner hot walls of the probe and deposit on the cold parts of the probe walls. So EM vapors, very important EM gasification products, may not be detected using this setup. Molecular beam mass spectrometric (MBMS) sampling[21] allows detection of radicals and other unstable species but disturbs the flame more strongly and therefore has reduced spatial resolution. We reported[19] the first use of MPT to study the solid propellant (SP) flame structure of ammonium perchlorate (AP) and polymethylmetacrylate. MPT was further applied to the study of EM flame structures with narrow combustion zones using AP and AP-based composite propellants. Figure 1 is a sketch of the MBMS system,[4–7] which has been used to examine the flame structures of AP, RDX, HMX, ADN, GAP and some composite SP. It includes a molecular beam sampling system, a time-of-flight mass spectrometer (type MSKh-4), a combustion chamber, a scanning system, a data acquisition system and an experiment controller based on CAMAC equipment and a computer. The sampling probe (item 3) is a 25-mm high cone with a 50-degree external angle, a 40-degree internal angle, and a 50–100 micron diameter orifice at the apex (at 1 atm). The probe produces a molecular beam, which passes to an ion source (item 4). The ignition spiral (12) is automatically removed from the combustion zone after ignition. The EM flame is scanned using a control system and a stepper motor (13) to move the burning strand (14) at a speed of less than 20 mm/s. A thermocouple (15) measures temperature profiles.

To study the flame structure at high pressure by MBMS, we use a quartz probe with an inner angle of 40 degrees and an orifice of 50 microns at 3 atm, 20 microns at 6 atm and wall thickness near the probe tip of 25 microns. We

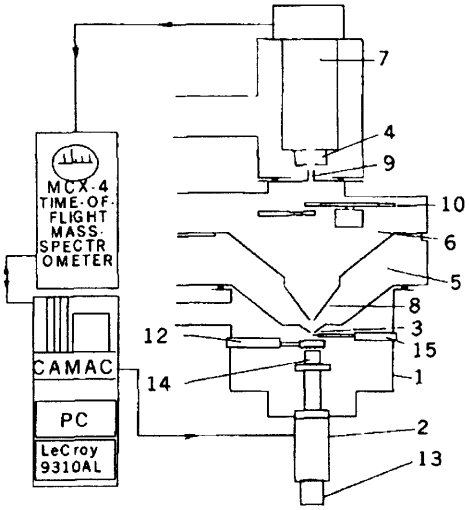

Fig. 1. MBMS system for studying the name structure of EMs with TOFMS.

visualize the combustion using a video camera (Panasonic NV-M3000EN). CAMAC equipment assisted the measurement of peak intensities of selected masses as a function of time. It is not always possible, however, to predict which peaks will be found in a mass spectrum. To reveal unpredictable peaks in the mass spectrum an oscilloscope (LeCroy 9310AL with a memory of 1 MB) was used. This allowed detection of singular mass spectra within short time intervals of 0.01 s. To stop data acquisition at the time of probe contact with the burning surface, a special device was designed and manufactured: an end switch of the stepper motor moving the sample to the probe was used as a sensor keeping a record of contact. Video recording of the ADN strand burning surface and probe was performed simultaneously with mass spectra recording. The synchronization of the two measurements was achieved by allowing the contacts of the stepper motor end switch to close at the moment of probe contact with the strand-burning surface. The latter was accompanied by light diode luminescence simultaneously with the stoppage of step frequency generator, which starts the oscilloscope. The light diode luminescence was recorded by video camera.

2.2. *Coupled Mass Spectrometric and Laser Technique*

The MPT technique was also developed by Litzinger *et al.*[8,9,22,23] to study laser-supported combustion (LSC) using a triple quadruple mass spectrometer[15] and an ionization energy of 22 eV. Laser-supported

combustion enables studies at lower pressures in which the chemical reaction zones in the EM flame are spread and the errors in flame concentration profiles measured by the probe are reduced. It is generally believed that the flame zone width should be greater than the probe tip dimensions. But, in LSC, one must ensure that the probe does not shield the burning surface from the laser, reducing the energy to the surface, and that the probe is not heated by the intercepted laser beam. This inadvertent heating may increase the rate of chemical reactions in the extracted sample.

Laser irradiation is widely used for the study of EM ignition. A recent paper by Yang *et al.*[24] is devoted to comprehensive analysis and modeling of laser-induced ignition of RDX. Generally, the only measured characteristics of laser-induced ignition are ignition delay and surface temperature of EM as a function of heat flow. Unfortunately there are no experimental data on the gasification products and species concentrations as functions of time. The available data[9,22] have been obtained using MPT and do not contain information about EM vapors in the narrow (0.1 mm) zone near the EM surface. This near-surface information is necessary for understanding the mechanism of EM ignition and its transition to combustion on a molecular level, and for development of comprehensive ignition and combustion models. We have described experiments for study of ignition and combustion of EMs supported by CO_2 laser irradiation using MBMS.[25] The tip of the probe was 100–150 microns from the sample surface. This distance is close to the value of the sampling shift Z_0 (see below). So the probe sampled the products evolving directly from the EM surface during its ignition and its combustion as a function of time. The beam of the laser made a small angle to the surface, excluding possible probe shielding of the EM surface from the laser beam. Positioning was controlled with the help of a video camera. The tip of the probe was heated to the temperature of the burning surface to prevent clogging of the sampling orifice by reaction products.

2.3. *Mass Spectrometric Technique for Studying the Kinetics and Mechanism of Thermal Decomposition of EMs and their Vapors*

Probing mass spectrometry can also be successfully applied to the study of kinetics and mechanism of the thermal decomposition of an EM and its vapors. The thermal decomposition of EM is one of the most important stages of its combustion; hence knowledge of the kinetics and reaction mechanism of EM thermal decomposition under different conditions (including the temperature at the burning surface) is

necessary for development of EM combustion models. Such information can result from using Rapid-Scan FTIR spectroscopy, SMATCH/FTIR, and T-Jump/FTIR — all methods developed by Brill[26] and by the method of differential mass-spectrometric thermal analysis (DMTA) developed in our laboratory.[27] These methods give information about the products of EM decomposition including EM vapors (e.g., the molecules HMX, RDX, etc.) as well as their rates of evolution. We have described the setup for mass spectrometric investigations (e.g., MBMS) of the kinetics of EM thermal decomposition under the non-isothermal conditions approximately similar to those present in the condensed phase in the vicinity of the EM burning surface.[27] The EM sample was applied to a metal ribbon located in flow reactor near the tip of the probe and heated by electrical current at 100–1000 K/s. This technique also can be used for obtaining calibration coefficients for EM vapors.

3. Validating the Method of Probing Flames with Narrow Combustion Zones

Quantitative results of the mass spectrometric probing technique for EM flame structure depend on the performance of the probe. Detailed studies[28–31] have been carried out to validate the probe method when the ratio of the flame zone width, L_b, to the probe tip outside diameter, d, is close to one. The studies were made for a preheated ($T = 533$ K) AP flame[32] where the burning zone was about 0.1 mm wide at 0.6 atm. Distortions caused by the probe can be divided into external and internal ones: the external ones being hydrodynamic and thermal. The probe acts as a sink for matter and heat, which causes distortions of temperature and species concentration profiles.[33,34] Errors were determined[28,29,35] by measuring perturbations in the velocity field in one-dimensional gas flows using submicron particles and a pulsed laser. The flow starts deviating from one-dimensional type at a distance depending on the sampling factor, which is defined by the equation $\alpha_0 = 4Q/\pi d_0^2 v_0$.

Here Q is the sink flow rate, d_0 is the probe orifice diameter, and v_0 is the flow velocity. The velocity fields and stream lines near the orifice of a probe have been calculated from Rosen's disk sink model.[33] This model can be used to evaluate measurement errors. Probe-error estimates have also been carried out for a real flame. A preheated AP flame with $L_b \sim 0.1$ mm was used, but we were unable to find reliable data on the AP flame chemical structure. Model experiments were, therefore, performed with a methane-air flat flame with argon additive having a 0.5 mm burning zone width. A

special quartz probe was used (subsequently referred to as a macroprobe) with an outside tip diameter equal to the flame zone width of 0.5 mm and with a probe orifice of $d_0 = 0.012$ mm. This probe and flame were similar in such dimensionless parameters as $d_0(\alpha_0)^{0.5}/L_b, L_b/d \approx 1$ and $Re_d \approx 1$ to those used in the case of the AP flame (Re_d is the Reynolds number of the flow determined from the probe outside diameter). According to similarity theory, the equality of these numbers for the model flame and probe and the AP flame and real probe allows us to use the results from the former to study the latter.

The following methods were applied to study the structure of the model flame: (1) microthermocouple technique (MT) using Π-shaped platinum–platinum/rhodium thermocouples (wire diameter of 0.02 mm) for measuring temperature profile; (2) probe mass-spectrometry measuring methane concentration profiles by macroprobe and quartz microprobe with $d_0 = 0.06$ mm, $d = 0.12$ mm; (3) Spontaneous Raman Scattering (SRS) spectroscopy for measuring methane and nitrogen concentration profiles. The comparison of the results of measuring methane concentration profiles in the model flame by probing methods and non-intrusive diagnostics showed that the error of the probe technique in finding concentrations at the burning surface was less than 10%. When the tip of the probe diameter was reduced 7 times, the change in concentration was about 15%. Concentration profiles of methane measured with a probe agree within 15% with the undisturbed profiles, if the first profile is shifted toward the burner by a value close to Z_0, the calculated shift of the sampling point with respect to the unperturbed flow. Calculations[35] based on simplified assumptions of the flame and flow perturbations (using Rosen's model[33]) provided the following values: $Z_0 \approx 0.4d_0(\alpha_0)^{0.5}$ and $\Delta \approx 0.3d_0(\alpha_0)^{0.5}$, where Δ is a sampling-zone width representing spatial-sampling resolution. At mass-spectrometric study of preheated AP flame structure d_0 was 0.012 mm and $\alpha_0 = 75$. After applying appropriate corrections for the sampling point on the concentration profiles (Z_0 shift), the error in finding concentrations by the probe method was less than 15% of its maximal value. The sampling zone width was within ±15% of the AP flame zone width. This error is reasonably small for quantitative modeling of AP flame structure data. We note, however, that Smith[36] gives other formulas for the shift.

In judging these experiments, one must be aware that the thermal disturbance of a flame by a probe strongly depends on the shape, wall thickness, and composition of the probe. Specification of these probe characteristics is frequently omitted in published work. Estimation of the thermal disturbances should be carried out by comparison of temperature profiles in a flame measured by thermocouples located both close to the tip of a probe and far from it. If the difference in these profiles is small, the thermal disturbances of the flame by the probe is likely to be small. To reduce thermal disturbances, one should use probes made of quartz or alumina, with an angle of opening of a cone less than 30–40 degrees and with thin (about 100 microns) walls, especially near the tip of the probe. Making these probes is difficult. Large wall thickness may be the cause of significant disturbances reported in some work.[8,38] Composition distortions in MBMS sampling has also been considered and discussed by Knuth.[39]

Validations of the MBMS method for determination of product composition of SP combustion at high temperatures and pressures (40 atm) typical of combustion chambers of rocket motors have been reported in Refs. 40–42. Estimation of internal distortions of sample inside-probe and skimmer were performed by the numerical solution of the full set of unsteady Navier–Stokes equations for axially-symmetric flows of compressible gas. The combustion products of stoichiometric mixtures of ammonium dinitramide (ADN)–polycaprolactone (pPCLN) at 4 MPa were chosen as the object of investigation. The gas dynamics and chemical kinetics were simulated to assess the correctness of sampling. We showed that, during the sampling from flames, the relative change in concentrations for most of the stable species does not exceed 3% and, for H_2 and O_2, it does not exceed 12%. Results of experiment and calculation are in good agreement.

4. Flame Structure of AP and AP-Based Composite Propellants

The homogeneous condensed mono-propellants: AP, RDX and ADN have been examined in detail. They have simple chemical structures, so they provide good models for studying combustion mechanisms. They are also the main components of commonly-used composite solid propellants so knowledge of their combustion mechanisms is essential to developing composite-solid propellant combustion models.

An AP flame preheated to 533 K was studied at 0.6 and 1 atm using MPT[32] and MBMS.[21] Figure 2 presents the results of some peak intensity profile measurements obtained with MBMS probing of an AP flame preheated to 533 K at 1 atm.[21] These experiments showed detection of mass peaks for m/e equal to 83 and 100 — characteristic of perchloric acid. Thus, these experiments provided the experimental support of the hypothesis that perchloric acid is the main AP gasification product in the combustion wave and plays a key role in the AP combustion mechanism. This result laid the

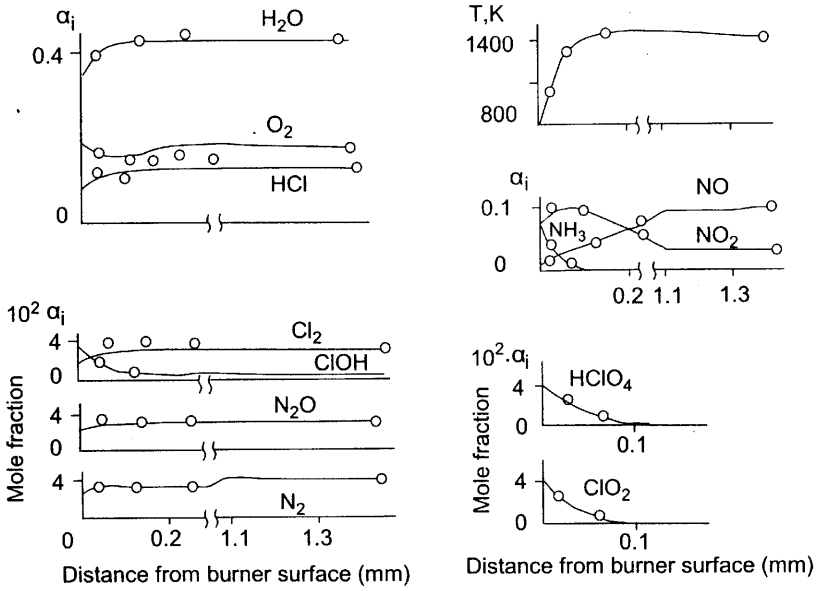

Fig. 2. AP flame structure (points are for experiment and lines are for calculation).

foundation for modern models of the combustion of AP. Chlorine dioxide and fragmentary ions of perchloric acid contribute to mass peak 67. We estimate that, at $L = 0$ to 0.05 mm, the contribution of perchloric acid to the intensity of mass peak 67 is about 50%. This means that the concentration of chlorine dioxide and perchloric acid are approximately equal near the burning surface.

Because of this near-equality, when analyzing MPT data, we assumed that half of the intensity of mass peak 67 came from chlorine dioxide in the flame and the other half from chlorine dioxide formed by heterogeneous catalytic decomposition of perchoric acid on the probe walls. Radicals, like HO_2, also recombined on the probe walls. Other species concentrations were determined using the measured calibration coefficients of individual species and mass-peak intensities obtained using MPT to study AP flames at 0.6 atm and 533 K. The ratio between the intensity of the perchloric acid peaks with m/e 83 and those of chlorine dioxide with m/e 67 (the latter being obtained with regard to the fact that the peaks with m/e 83 from perchloric acid contributes to the peaks with m/e 67) is shown in Table 1. This ratio (the intensity of the perchloric acid peaks with m/e 83 is equal to those of chlorine dioxide with m/e 67) was used when correlating the data obtained in setup No. 1, under which conditions chloride dioxide resulting

Table 1. Species mass peaks intensities (in relative units) at different L in AP flame (a setup with molecular-beam sampling).

m/e	L (micron)					
	0	50	100	150	200	250
83	230	140	65	10	0	0
67	290	280	190	90	20	0
52	310	270	230	160	80	0
51	200	180	130	90	30	0

from heterogeneous catalytic decomposition of perchloric acid on the probe walls into ClO_2 and HO_2 contributes to a peak with m/e = 67. Using the results of measuring calibration coefficients by individual species and mass peak intensities of the species obtained in the experiments in setup No. 1 studying AP flame structure at 0.6 atm (533 K), species concentrations were found. Profiles of species concentrations and temperature versus the distance from the burner surface L are presented in Fig. 2. Concentration profiles in an AP flame show the following two-zone structure: in a narrow (~0.1 mm wide) zone, NH_3, $HClO_4$ and ClO_2 concentrations fall and NO_2 concentrations rise, and in the next wide (~1.5 mm wide) zone NO_2 concentrations fall while NO and O_2 concentrations rise. Figure 2 also represents modeling results for the same flame structure (lines)[43,44] performed using a mechanism incorporating 80 reactions. The reduced mechanism is presented below.

$$ClO_3 = ClO + O_2, \quad (1)$$
$$ClO_2 + Cl = 2ClO, \quad (2)$$
$$2ClO = Cl_2 + O_2, \quad (3)$$
$$ClO + NO = Cl + NO_2, \quad (4)$$
$$ClO + NH_3 = NH_2 + ClOH, \quad (5)$$
$$OH + HCl = H_2O + Cl, \quad (6)$$
$$Cl + O_2 + M = ClO_2 + M, \quad (7)$$
$$HNO + O_2 = NO_2 + OH, \quad (8)$$
$$NH_2 + O_2 = HNO + OH, \quad (9)$$
$$ClOH + OH = ClO + H_2O, \quad (10)$$
$$NH_3 + Cl = NH_2 + HCl, \quad (11)$$
$$OH + HNO = H_2O + NO, \quad (12)$$
$$HClO_4 = OH + ClO_3, \quad (13)$$
$$HClO_4 + HNO = ClO_3 + NO + H_2O, \quad (14)$$
$$NO_2 + NO_2 = O_2 + 2NO, \quad (15)$$
$$NH_3 + OH = NH_2 + H_2O, \quad (16)$$
$$HClO_4 + HNO = ClO_2 + NO_2 + H_2O. \quad (17)$$

Satisfactory agreement between the calculation and experimental results provides evidence for the suggested mechanism. Subsequent work provides a revised mechanism.[45] The obtained results were used when developing an AP combustion model.[46–49] Lin *et al.* have investigated unimolecular decomposition of perchloric acid and the related $OH + ClO_3$ reaction[50] as well as ClO_x reactions and the reaction of OH with ClO by *ab initio* molecular orbital and variational transition state theory calculations. It allows us to refine chemical kinetics models of reactions in AP flames.

The flame structure of composite propellants based on AP (particle size less than 50 micron) and HTPB was studied at subatmospheric pressures in setup No. 1 with MPT and modeling.[51–53] Eighteen stable species (HCl, H_2O, CO, NH_3, CO_2, HClO, NO, O_2, H_2, NO_2, N_2O, N_2, C_4H_6, C_2H_2, ClO_2, Cl_2, HCN, $HClO_4$) were detected in the flame zone. No mass peaks 83 and 100 were found but $HClO_4$ concentration was determined as it was for the AP flame. Profiles of species concentrations and temperature in flames of model composition HTPB/AP (16/84) at 0.08 atm are shown in Fig. 3.

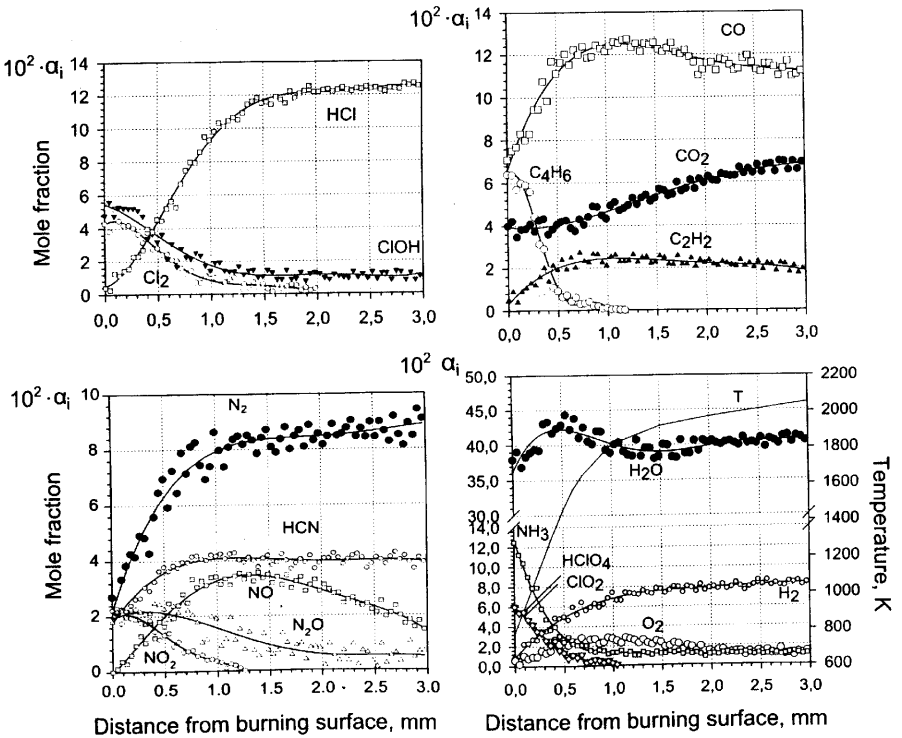

Fig. 3. AP/HTPB flame structure.

Kinetics model includes 58 reactions and 35 species. Satisfactory agreement between the experimental and calculated data was achieved. The reactions of oxidation of ammonia and HTPB destruction products with perchloric acid decomposition products (ClO_2, ClOH, ClO, etc.) are the main reactions in the flame of composite propellants based on AP and HTPB. The chemical transformations in the AP/HTPB flame is shown in Scheme 1.

The data analysis of flame structure of composite propellant based on AP and HTPB (especially rich formulations) at low pressure indicates that oxidation of hydrocarbon binder destruction products occurs in the flame

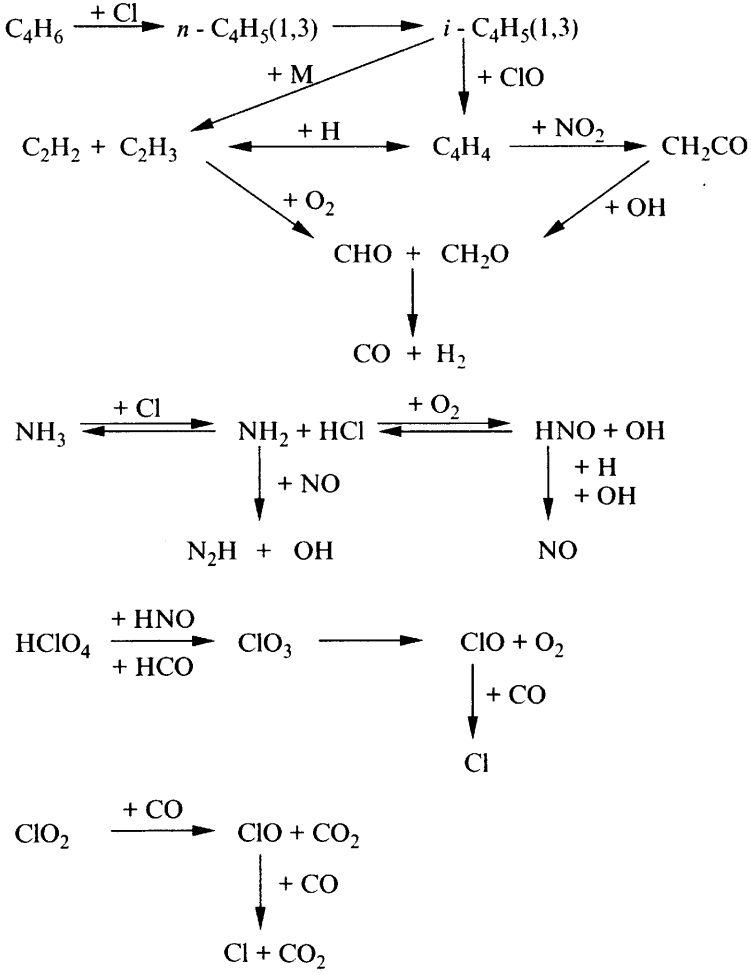

Scheme 1.

much faster than ammonia oxidation. The obtained data were used when developing a combustion model of AP composite propellants.[54] The flame structure of a sandwich system consisting of alternating laminas of AP and polymerized mixtures of fine-grained AP and polybutadiene binder ("base" lamina) was studied in Refs. 55–57. The profiles of concentrations for 17 stable species and of temperature for three cross-sections corresponding to the middle of the AP lamina, to the middle of the "base" lamina, and to the interface between the laminas have been determined. The hypothesis assuming the existence of three types of flames at the boundary of the AP particle and the binder in composite SP have been verified and confirmed experimentally. It was observed that the concentration gradient of fuel species at the burning surface of the AP is directed towards the burning surface. A modeling of the flame structure sandwich system has been carried out.

The ignition of the pseudo-propellants AP/HTPB and AP/PMMA and its transition to the combustion under CO_2–laser radiation was investigated at 0.1 MPa of argon using MBMS.[25] The initial distance between the orifice of the probe and the surface of the propellant was equal to 0.1–0.15 mm. The perchloric acid and ammonia, the key species of SP gasification during its ignition and combustion were detected. In addition, the dependencies of mass peak intensities of gasification products on time during and after propellant ignition were determined. The data on propellant gasification products during the ignition with simultaneous measurement of temperature of gas phase near the burning surface were obtained in some experiments.

5. RDX and HMX Flame Structure

The results of studying the flame structure in the high temperature zone of the RDX flame at 0.5 atm[28,58] using the MBMS technique are shown in Fig. 4. The burning surface was identified, with allowance for the sampling shift Z_0 calculated from the above mentioned formula ($\alpha_0 = 70$, $d_0 = 0.1$ mm). These results show that the key species in the RDX high temperature flame zone are NO and HCN. The main reaction in the high temperature zone of the RDX flame is the reaction HCN + NO and not $CH_2O + NO_2$ as was previously postulated.[59] Figure 4 also shows calculated profiles of mole fraction from the results of Ermolin *et al.*[58] The calculations are in satisfactory agreement with the experimental data. List of the

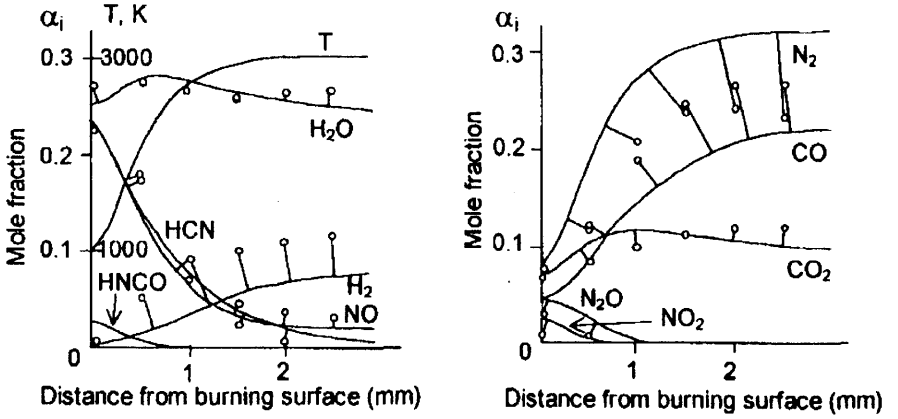

Fig. 4. Temperature and species mole fraction profiles in RDX flame at 0.5 atm (points are for experiment and solid line for modeling).

most important reactions in high temperature flame zone selected from the full mechanism is presented below.

$$HCN + OH = CN + H_2O, \quad (18)$$
$$CN + NO = CO + N2, \quad (19)$$
$$HCN + OH = NH_2 + CO, \quad (20)$$
$$NO_2 + H = NO + OH, \quad (21)$$
$$NO + N = N_2 + O, \quad (22)$$
$$NO + H + M = HNO + M, \quad (23)$$
$$2HNO = H_2O + N_2O, \quad (24)$$
$$H_2 + O = OH + H, \quad (25)$$
$$CO_2 + M = CO + O + M, \quad (26)$$
$$H_2O + O = 2OH, \quad (27)$$
$$CO_2 + H = OH + CO, \quad (28)$$
$$NH + OH = N + H_2O, \quad (29)$$
$$NH + H = N + H_2, \quad (30)$$
$$NH_2 + OH = H_2O + NH, \quad (31)$$
$$OH + H_2 = H_2O + H, \quad (32)$$
$$NH_2 + NO = N_2H + OH, \quad (33)$$
$$N_2H + NO = HNO + N_2, \quad (34)$$
$$OH + N_2O = N_2 + HO_2, \quad (35)$$
$$HO_2 + NO = NO_2 + OH, \quad (36)$$
$$NH + NO = N_2 + O + H. \quad (37)$$

Melius' mechanism[60,61] provided better agreement with the experimental results as compared with that of Ermolin *et al.*[58] Later Ermolin[62] refined the mechanism and obtained better agreement with experiment than in Ref. 58. The obtained data have also been used by other researchers[63–66] when developing and validating detailed RDX combustion mechanisms and models. The analysis of experimental data[28] and Melius' model[60,61] predict the existence of a narrow "cool" flame zone (less than 0.1 mm at 0.5 atm), where RDX vapor decomposition takes place.

The flame structure at RDX self-sustained combustion at 1 atm has been studied using planar laser induced fluorescence (PLIF) and UV/vis absorption spectroscopy.[14]

Profiles of NO, NO_2, OH, NH, CN concentrations and of temperature have been measured. Some later similar measurement and modeling have been done in Ref. 67 and compared with data of Ref. 14. Results[67] of modeling RDX self-sustained combustion are in a good agreement with modeling results of Lian and Yang.[63]

Low temperature flame zones in RDX and HMX flames have been studied by different authors[14,68,69] mainly using thin thermocouples. Some of the investigators reported a plateau on the temperature profile near the burning surface of a temperature of ~1000 K. This plateau would provide support for the hypothesis of a narrow zone in "cool" flames where RDX or HMX vapor decomposition takes place. Other researchers[69,14] however did not confirm this fact. The study of a narrow zone (~0.1 mm wide) in an RDX flame using MPT with a probe having an orifice of about 0.01 mm could lead to erroneous conclusions. This is due to the fact that in this case the RDX vapors would be hardly detectable through their possible heterogeneous catalytic decomposition at the microprobe walls (similarly to $HClO_4$ decomposition at microprobe walls in AP flame). Due to the difficulties in MBMS study of flame zones less than 0.1 mm wide, there is to date no direct experimental evidence of the existence of RDX vapor decomposition in RDX flames. Nevertheless, in combustion models the existence of such a zone is supposed. This problem is to be solved in the future.

There is much that is common to HMX and RDX flame structures, but there are differences as well. As is apparent from profiles of mass peak intensities in an HMX flame at 1 atm,[6,70] and sandwich systems based on HMX,[55,56] two clearly defined subzones are seen in the high temperature zone of the HMX flame. CH_2O and N_2O decomposition takes place in the first one, while HCN oxidation with nitrogen oxide, as in the RDX flame, takes place in the second. It should be noted that NO_2 and CH_2O were also found in the RDX flame at 0.5 and 1 atm. However, mass peaks at intensities of 46 (N_2O) and 29 (CH_2O) were detected in those cases to a much lesser extent. These observations are also confirmed by results of spectroscopic study.[14] The results obtained for HMX flame structures were used when developing the HMX combustion model.[71]

CO_2 laser-assisted combustion of RDX and HMX at 1 atm and the structure of a flame were studied in Refs. 14, 16, 23, 38, and 72–75. As comparison of temperature profiles in flames at self-sustaining (flame 1) and laser-assisted (flame 2) combustion shows, they strongly differ. In flame 2 there is a dark zone and two-stage form of temperature profile,[14] which is not observed in flame 1.[69] It is necessary however, to note the distinction in the form of the temperature profiles received in Refs. 14 and 23: there is no plateau on the temperature profile at a distance of 1–2 mm from a burning surface in Ref. 23, which was observed in Ref. 14. The basic chemical processes going on in a dark zone of width 0.5 mm, adjusting to a burning surface, are the reactions of HCN oxidation and NO_2 decomposition with NO formation. In the second luminous zone there is a further HCN oxidation with NO with formation of N_2 and CO. There are also contradictions in the CH_2O concentration in Refs. 23, 38, and 72. The results of modeling the RDX flame structure at laser-assisted combustion[38,62,66,75] do not correspond with the results of experiment. Similar situations can be seen in the case of HMX laser-assisted combustion.[73] There is not enough understanding in HMX laser-assisted combustion chemistry. One of the reasons for the contradictions in the received results of the study of RDX and HMX laser-assisted combustion is probably error connected with the use of a microprobe method, which results in strong thermal disturbance of a flame by a probe with thick walls, and catalytic decomposition of a sample on the internal walls of a hot probe. The differences in RDX and HMX flame structure in self-sustained and laser-assisted combustion support the suggestion that the chemical combustion mechanisms are different in these two processes. So it is not possible to apply the laser-assisted combustion model for the development of a combustion model for self-sustained combustion of EM.

6. Flame Structure of ADN and ADN-Based Propellants

ADN is a new energetic material which can be used as an oxidizer in solid rocket propellants.[76] It presents an alternative to ammonium perchlorate (AP), being an ecologically pure oxidizer in solid propellants. ADN is a simpler mono-propellant than AP and RDX, as defined both by the number of elements and by the possible intermediate and final combustion products. In the last few years several works devoted to the study of the ADN combustion mechanisms have been published.[22,27,77–84]

To understand the mechanism of the primary stage of ADN decomposition, and to study the mechanism and kinetics of secondary reactions of ADN decomposition products, two-temperature flow reactors combined with MBMS[27,85] and MPT[86] were used. ADN was heated at low pressure (6–10 torr) in the first reactor at temperature 350–410 K. Then decomposition products entered and reacted in the second reactor

at temperature 430–1170 K. Authors of Ref. 86 assumed that products of ADN decomposition in the first reactor are products of ADN dissociative sublimation: dinitraminic acid (DA) and ammonia. They measured and calculated concentrations of four species (NH_3, N_2O, H_2O, N_2) in products of thermal decomposition DA + NH_3 in the second reactor at 370–920 K using the suggested model, involving 152 reactions. They also developed a kinetic model for dinitraminic acid thermal decomposition at low pressure. Authors of Refs. 27 and 85, based on the detailed study of the mass spectrum of products of ADN decomposition in the first reactor as well as the mass spectra of DA and ammonia using MBMS, came to the conclusion that ADN evaporation takes place in the first reactor. ADN decomposition at 350–410 K in a flow reactor at 6–10 torr showed that more than 90% of ADN deposited on the cold walls of the tube at the exit of the flow reactor. Temperature dependence of ADN vapor pressure $\lg P = 18.32 - 8.09 \times 10^3/T$, P (torr), T (K) was determined. Sublimation (evaporation) heat is $\Delta H_{\text{subl}} = 37 \pm 3$ kcal/mole corresponding to this dependency, which is close to the calculated results, 38 kcal/mole, obtained in Ref. 87. From theoretical study it was suggested that the next mechanism of ADN thermal decomposition is:

$$\text{ADN}_\text{s} \xrightarrow{\Delta H = 38 \text{ kcal/mole}} \text{HN}_3[\text{HN}(\text{NO}_2)_2] \xrightarrow{\Delta H = 12\text{–}14 \text{ kcal/mole}} \text{NH}_3 + \text{HN}(\text{NO}_2)_2$$

The kinetics and mechanism of the secondary reactions of ADN vapor decomposition at 6 torr have been studied[85] using MBMS and modeling based on kinetic mechanism.[86] The additional experimental evidence of ADN evaporation has been obtained: NH_3 concentration increased in the temperature range 430 to 530 K. The authors of paper 86 did not notice this fact because they did not take into account the contribution of the fragmentary ion of ADN_v to the intensity of mass peaks 17 and 16. Also if ADN decomposition yielding DA and NH_3 was the first stage of the process, the temperature dependence of DA + NH_3 vapors would correspond to $\Delta H_{\text{subl}} = 25\text{–}26$ kcal/mole but not to $\Delta H_{\text{subl}} = 37 \pm 3$ kcal/mole. The rate constant of ADN_v dissociation $ADN_v + M \rightarrow NH_3 + HN(NO_2)_2 + M$ has been determined from experimental data $k = 3 \times 10^{12} \exp(-12000/RT)$, $\text{cm}^3\ \text{mole}^{-1}\,\text{s}^{-1}$. These conclusions are in good agreement with the data of Ref. 87. So the mechanism of ADN evaporation differs from that of other ammonium salts. In the case of ammonium perchlorate and ammonium nitrate, dissociative sublimation takes place, yielding ammonia and the corresponding acid. The obtained mass spectra

of ADN vapor allowed us to identify it in the "cool" flame zone at 1 and 3 atm and to measure its concentration.

The temperature distribution in the wave of ADN combustion has been measured using thin thermocouples in a wide pressure range which has revealed several burning zones. The composition of ADN combustion products has been determined by the authors of paper 79 at 0.26–0.78 atm. But the purity of ADN in this study[79] was very bad. ADN combustion mechanisms suggested in Refs. 27, 78, 79, 83 are different. Thus, it is suggested in Refs. 79 and 83 that ADN reactions in the condensed phase result in ammonium nitrate. The dissociation of ammonium nitrate yielding NH_3 and HNO_3 controls the temperature of ADN burning surface and, therefore, the burning rate. Another mechanism has been discussed in Refs. 27 and 82. It is based on the results of studying the chemical structure of the ADN flame at 1–6 atm using an MBMS and the microthermocouple technique.[27] The flame structure was found to involve three zones. At 1–3 atm a luminous flame zone was not observed. The burning rate at 1–6 atm is controlled by reactions in the condensed phase. At 3 atm a "cool" flame zone adjacent to the burning surface was found. The width of this zone is about 1–1.5 mm. The following species have been identified in the "cool" flame zone: HNO_3, NO_2, N_2O, NH_3, NO, N_2, H_2O and ADN vapor. The ratio between the mass peak intensities in the mass spectra of samples taken from the zone close to the ADN burning surface at 3 atm and those of ADN decomposition products[27,85] are in reasonable agreement.

The analysis of the mass spectra of the samples taken from the zone near the ADN burning surface at 3 atm has shown that gaseous ADN and dinitraminic acid are the key reactants in the near-surface zone. The product composition near the ADN burning surface has been determined. Gaseous ADN and dinitraminic acid decomposition in the near-surface zone results in a temperature rise of about 150 K. The second high temperature zone was found to be 6–8 mm from the ADN burning surface at 6 atm (Fig. 5). The main reaction in this zone is ammonia oxidation by nitric acid, while the temperature rise is 500 K. The combustion temperature is 1400 K and the combustion products are H_2O, NO, N_2O, N_2. The ADN flame structure studied at a pressure of 40 atm[80] revealed the presence of three zones of chemical transformations. The first, a low-temperature ~0.1 mm wide zone associated with the rise in temperature from 640 to ~970 K which is similar to the ~1 mm wide zone obtained in ADN burning at 3–5 atm. The second is a 1 mm wide zone associated with the rise in temperature from 970 to ~1370 K which is similar to the ~11 mm wide zone found in the burning of ADN at 5–6 atm. The third zone is at a distance of ~1 to

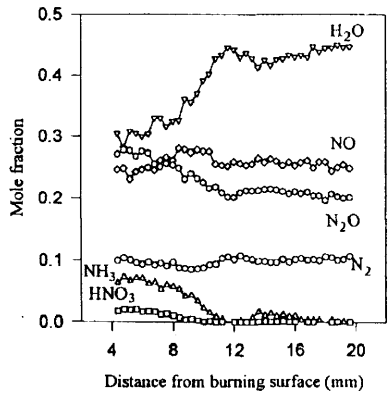

Fig. 5. Species mole fraction profiles in ADN flame at 6 atm, experimental results.

Table 2. Product composition in ADN flame.

P (atm)	L (mm)	NH_3	H_2O	N_2	NO	N_2O	ADN_v	HNO_3	O_2
3	0.2	0.08	0.30	0.08	0.19	0.24	0.03	0.08	0
6	4.4	0.07	0.30	0.10	0.23	0.28	0	0.02	0
40	1.5	0	0.42	0.18	0.21	0.14	0	0	0.05

6 mm from the burning surface and is associated with N_2O consumption. The temperature in it increases from 1370 to 1770 K. The width of the third zone depends on the ADN burning rate. ADN combustion product compositions at 3 and 6 atm at different distances (L) from the burning surface are shown in Table 2. The temperatures, product compositions measured at the distances $L = 0.2$, 4.4 and 1.5 mm at 3, 6 and 40 atm and product mass flows were used as boundary conditions in the modeling of the ADN flame using CHEMKIN Code[88] and based on the developed mechanism (98 reactions and 22 species). Part of these reactions and their rate constants have been calculated and suggested by Park *et al.*[86] The results of temperature and species concentration profile calculations[80,82,84] are in a good agreement with experimental data. The calculation has also shown the existence of a fourth zone at higher pressures, where nitric oxide decomposes to nitrogen and oxygen with a temperature rise to a value (~2100 K) close to the thermodynamic equilibrium temperature. The results of sensitivity analysis for most of the important reactions in all flame zones are presented in Table 3. ADN combustion chemistry is described in Scheme 2. The obtained data is applicable for developing an ADN combustion model.

Table 3. The most important reactions in ADN flame.

Zone number	Reaction
1	73. $NH_3 + OH = NH_2 + H_2O$
	111. $HN_3O_4 = HNNO_2 + NO_2$
	114. $HNNO_2 + NO_2 = HNO + NO + NO_2$
	134. $HNNO_2 + NO = HNNO + NO_2$
	135. $HNNO_2 + NO = HONO + N_2O$
	172. $ADN_v + M = NH_3 + HN_3O_4 + M$
2	36. $NO + OH(+M) = HONO(+M)$
	65. $NH_2 + NO = NNH + OH$
	66. $NH_2 + NO = N_2 + H_2O$
	73. $NH_3 + OH = NH_2 + H_2O$
	94. $HONO + OH = H_2O + NO_2$
3	101. $N_2O + NO = NO_2 + N_2$
4	105. $NO + NO = N_2 + O_2$

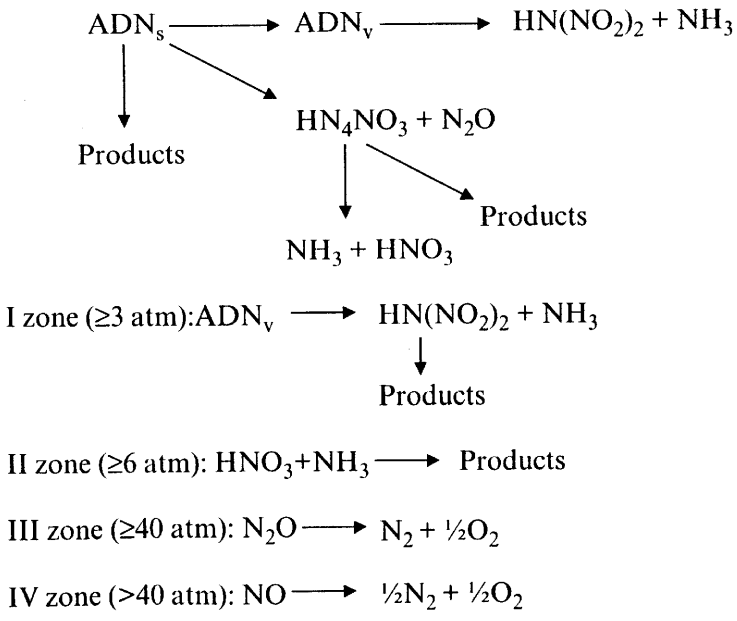

Scheme 2.

The flame structure of the composite pseudo-propellants based on ADN and several binders, such as PCL, HTPB and glycidyl azide polymer (GAP), was studied using MBMS.[81,89–92] Combustion of stoichiometric compositions based on ADN and PCL has been studied in details.[89,91,92] The combustion of PCL/ADN (10,92/89,08) and HTPB/ADN (3/97) propellants at 1 atm is jet-like in nature. Video-recording demonstrated the presence of several brightly luminous jets of about 0.5–1 mm in diameter at the burning surface, disappearing at one site and appearing at another with a lifetime of 0.2 s. The spatial heterogeneity and non-stationary nature of the propellant combustion process is in agreement with mass spectrometric and temperature measurements.

The videotape recording of ADN/PCL combustion showed that a dark zone exists near the burning surface. The width of the dark zone varies from ~1 mm (near the bottom of the torch) to 3–4 mm (in the region between torches). Thermocouple measurements revealed the existence of three zones in the flame (1) the narrow dark zone adjacent to the burning surface (width of the zone ~0.2–0.3 mm), where the temperature grew from ~600 to ~1150 K, (2) the dark zone (width of the zone is ~0.5 to ~3 mm) where the temperature slightly increased from 1150 to 1450 K, (3) the luminous zone (torch), where the temperature increased to 2600 K at the distance of 4–8 mm. Compositions of the combustion products in the luminous and dark flame zones of propellant ADN/PCL (molecular weight PCL 1250) are presented in Table 4. The temperature of the combustion products in the luminous zone, which is equal to 2600 K, is slightly less than the calculated equilibrium temperature (2695 K), i.e. 100% completeness of combustion is not achieved. The presence of NO in combustion products confirms this conclusion. The element balance in the luminous

Table 4. Concentrations (in mole fractions) of species and temperature in flame of propellant ADN/PCL at 1 atm and of ADN at 6 atm.

	T (K)	H_2O	N_2	N_2O	NO	NH_3	HNO_3	H_2	CO	CO_2	O_2
Luminous zone (exp)	~2600	0.39	0.32	0	0.10	0	0	0.03	0.02	0.12	0.02
Thermodynamic calc.	2695	0.40	0.34	0	0.01	0	0	0.03	0.05	0.09	0.03
Dark zone (exp)	~1120	0.32	0.11	0.20	0.20	0.04	0.01	0.01	0.02	0.08	0.01

zone was in satisfactory agreement (±5%) with that in the propellant. The calculated deficiency of carbon in the combustion products determined in the dark zone is equal to ~50% of the initial amount. This fact indicates that identification of carbon-containing products in the dark zone was incomplete. Besides, peaks of the following unidentified masses in the mass spectrum of species near the burning surface of the propellant have been obtained: 55, 57, 60, 67, 69, 70, 71, 73, 79, 81, 95, 108, 115. It was assumed that masses from 55 to 115 are responsible for the decomposition of PCL.

For propellant HTPB/ADN (3/97) at 6 atm, video-recording near the burning surface revealed a dark zone of ~0.3 mm, which was in agreement with the data obtained when studying the flame structure of ADN-based sandwiches.[90] The dark zone width increases up to 1.5 mm as pressure is reduced to 1 atm. Thermocouple investigations have shown temperature fluctuations of about ±400 K at 1 atm in the flame zone within 1.5–4 mm from the burning surface. Along with the temperature fluctuations, variations in the intensities of mass peaks 17 (NH_3), 28 (CO, N_2), 30 (NO), 46 (HNO_3, NO_2), 44 (CO_2, N_2O) take place. The values for mass peak relative intensities of combustion products near the burning surface of ADN/HTPB 97/3 propellant and pure ADN at 1 atm are close. Analyzing the data on mass peaks intensities in the mass spectra of samples near a burning surface of ADN and ADN/HTPB at 1 atm, one can suggest that pure ADN combustion products are mainly found in the dark zone of propellant combustion, and that luminous jets are formed in the gas phase when ADN decomposition products are mixed with HTPB decomposition products. One of the explanations for the presence of luminous jets with a mean size of ~0.5–1 mm at the burning surface may be the agglomeration of small ADN and (or) binder particles into larger ones at the burning surface. The combustion product composition of composite propellant ADN/HTPB 97/3 at 1 atm approaches the product composition of pure ADN combustion at 6 atm, in the content of nitrogen-containing components. So ADN-HTPB interaction in flame provides an increase in final temperature and ADN combustion completeness.

7. Conclusions

By the example of the study of the flame structure of AP, RDX, HMX, ADN and some propellants, the probing mass-spectrometry procedure has been shown to be an indispensable method providing important information on

EM chemical combustion mechanisms. Although it is limited to some extent by pressure, flame zone width and other considerations, the results obtained with its aid have successfully been used to understand the chemical reaction mechanisms of EM combustion and to develop combustion models. Further application of this method, as well as other spectroscopic and thermocouple methods, will allow a refined and widened understanding of EM combustion mechanisms.

References

1. T. Edwards, *Solid Propellant Flame Spectroscopy*, Air Force Astronautics Laboratory, AFAL-TR-88-076, Edwards AFB, CA (1988).
2. Y. B. Zel'dovich, *J. Exp. Theoret. Phys.* **12**, 498 (1942), in Russian.
3. R. M. Fristrom, *Flame Structure and Processes* (Oxford University Press, New York, 1995).
4. O. P. Korobeinichev, *Combust. Explos. Shock Waves* **23**, 565 (1988).
5. O. P. Korobeinichev, *Pure Appl. Chem.* **65**, 269 (1993).
6. O. P. Korobeinichev, L. V. Kuibida, A. A. Paletsky and A. A. Chernov, *Combust. Sci. Technol.* **113–114**, 557 (1996).
7. O. P. Korobeinichev, in *Solid Propellant Chemistry, Combustion and Motor Interior Ballistics*, Progress in Astronautics and Aeronautics, Vol. 185, eds. V. Yang, T. B. Brill and W. Z. Ren (AIAA, Reston, VA, 2000), p. 335.
8. T. A. Litzinger, Y. J. Lee and C. J. Tang, in *Solid Propellant Chemistry, Combustion and Motor Interior Ballistics*, Progress in Astronautics and Aeronautics, Vol. 185, eds. V. Yang, T. B. Brill and W. Z. Ren (AIAA, Reston, VA, 2000), p. 355.
9. T. A. Litzinger, Y. J. Lee and C. J. Tang, in *Proc. Workshop on the Application of Free-Jet, Molecular Beam, Mass Spectrometric Sampling*, National Technical Information Service (NTIS), US, Department of Commerce, Springfield, VA, 1994, p. 128.
10. J. A. Vanderhoff, M. W. Teague and A. J. Kotlar, *Absorption Spectroscopy Through the Dark Zone of Solid Propellant Flame*, Ballistic Research Lab. Rept. BRL-TR-3334 (1992).
11. T. P. Parr and D. M. Hanson-Parr, in *Non-Intrusive Combustion Diagnostics*, eds. K. K. Kuo and T. P. Parr (Begell House Publishing, Inc., New York, 1994), p. 517.
12. J. H. Stufflebeam and A. C. Eckbreth, *Combust. Sci. Technol.* **66**, 163 (1989).
13. T. P. Parr and D. M. Hanson-Parr, in *26th Symp. (Int.) Combustion* (The Combustion Institute, Pittsburgh, PA, 1996), p. 1981.
14. T. P. Parr and D. M. Hanson-Parr, in *Decomposition, Combustion and Detonation of Energetic Materials*, Proc. Mat. Res. Soc., Vol. 418, eds. T. B. Brill, T. P. Russell, W. C. Tao and R. B. Wardle (1996), p. 207.
15. S. H. Modiano and J. A. Vanderhoff, in *26th Symp. (Int.) on Combustion* (The Combustion Institute, Pittsburgh, PA, 1996), p. 2017.

16. T. Parr and D. Hanson-Parr, in *Solid Propellant Chemistry, Combustion and Motor Interior Ballistics*, Progress in Astronautics and Aeronautics, Vol. 185, eds. V. Yang, T. B. Brill and W. Z. Ren (AIAA, Reston, VA, 2000), p. 381.
17. A. A. Zenin, *Fiz. Goreniya Vzryza* **2**, 67 (1966), in Russian.
18. C. A. Heller and A. S. Gordon, *J. Phys. Chem.* **59**, 773 (1955).
19. O. P. Korobeinichev and A. G. Tereshchenko, *Doklady Akademii Nauk USSR* **231**, 1159 (1976), in Russian.
20. O. P. Korobeinichev, I. N. Skovorodin, E. L. Emel'anov, K. P. Kassheev, S. V. Polozov, A. G. Tereschenko, L. V. Kuibida and V. V. Ivanov, *Byulleten' Izobreteney i otkrytiy* **30** (1980), in Russian.
21. O. P. Korobeinichev and L. V. Kuibida, in *Flames, Lasers and Reactive Systems*, Progress in Astronautics and Aeronautics, Vol. 88, eds. J. R. Bowen, N. Manson, A. K. Oppenheim and R. I. Soloukuin (AIAA, New York, 1982), p. 197.
22. B. L. Fetherolf and T. A. Litzinger, in *29th JANNAF Combustion Meeting*, Vol. 2, CPIA Publication 593, (1992), p. 329.
23. Y. J. Lee, C. J. Tang and T. A. Litzinger, *Combust. Flame* **117**, 600 (1999).
24. Y.-C. Liau, E. S. Kim and V. Yang, *Combust. Flame* **126**, 1680 (2001).
25. A. G. Tereshchenko, O. P. Korobeinichev, A. A. Paletsky and L. T. DeLuca, in *Rocket Propulsion: Present and Future*, ed. L. T. DeLuca (Grafiche GSS, Bergamo, Italy, 2003), paper 24.
26. T. B. Brill, *Prog. Energy Combust. Sci.* **18**, 91 (1992).
27. O. P. Korobeinichev, L. V. Kuibida, A. A. Paletsky and A. G. Shmakov, *J. Propul. Power* **14**, 991 (1998).
28. O. P. Korobeinichev, L. V. Kuibida, V. N. Orlov, A. G. Tereshchenko, K. P. Kutsenogii, R. V. Mavliev, N. E. Ermolin, V. M. Fomin and I. D. Emel'yanov, in *Mass-Spektrometriya i Khimia Kinetika*, ed. V. Tal'rose (Nauka, Moscow, 1985), p. 73, in Russian.
29. O. P. Korobeinichev, A. G. Tereshchenko, I. D. Emel'yanov, L. V. Kuibida, V. N. Orlov, R. V. Mavliev, K. P. Kutsenogii, A. L. Rudnitskii, S. Yu. Fedorov, N. E. Ermolin and V. M. Fomin, *Probe Mass-Spectrometry for Condensed System Flames Having Narrow Combustion Zones* (Institute of Chemical Kinetics and Combustion, Novosibirsk, 1985), preprint No. 14, in Russian.
30. O. P. Korobeinichev, A. G. Tereshchenko, I. D. Emel'yanov, A. L. Rudnitskii, S. Yu. Fedorov, L. V. Kuibida, V. V. Lotov and V. N. Orlov, *Combust. Explos. Shock Waves* **21**, 524 (1985).
31. I. D. Emel'yanov, O. P. Korobeinichev, A. G. Tereshchenko and L. V. Kuibida, *Combust. Explos. Shock Waves* **22**, 168 (1986).
32. N. E. Ermolin, O. P. Korobeinichev, A. G. Tereshchenko and V. M. Fomin, *Combust. Explos. Shock Waves* **18**, 36 (1982).
33. P. Rosen, *Potential Flow of Fluid into a Sampling Probe*, Applied Physics Laboratory, Johns Hopkins University, Rept. CF-2248 (1954).
34. V. V. Dubinin, B. Ya. Kolesnikov and G. I. Ksandopulo, *Fizika Goreniya i Vzryva* **13**, 920 (1977).
35. K. P. Kutsenogii, O. P. Korobeinichev, R. V. Mavliev and A. G. Tereshchenko, *Dokl. Akad. Nauk SSSR* **282**, 1425 (1985), in Russian.

36. O. Smith, in *Flame Structure and Processes*, ed. R. M. Fristrom (Oxford University Press, New York, 1995).
37. A. T. Hartlieb, B. Atakan and K. Kohse-Hoinghaus, *Combust. Flame* **121**, 610 (2000).
38. T. A. Lintzinger, B. L. Fetherolf, Y. J. Lee and C-J. Tang, *J. Propul. Power* **11**, 698 (1995).
39. E. L. Knuth, *Combust. Flame* **103**, 171 (1995).
40. O. P. Korobeinichev, A. G. Tereshenko, P. A. Skovorodko, A. A. Paletsky and E. N. Volkov, in *Proc. 18th ICDERS* (2001), paper 82-1.
41. A. G. Tereshenko, O. P. Korobeinichev, P. A. Skovorodko, A. A. Paletsky and E. N. Volkov, *Fiz. Goreniya Vzryza* **38**, 91 (2002), in Russian.
42. O. P. Korobeinichev, A. A. Paletsky, A. G. Tereshenko and E. N. Volkov, *J. Propul. Power* **19**, 203 (2002).
43. N. E. Ermolin, O. P. Korobeinichev, A. G. Tereshchenko and V. M. Fomin, *Combust. Explos. Shock Waves* **18**, 180 (1982).
44. N. E. Ermolin, O. P. Korobeinichev, A. G. Tereshchenko and V. M. Fomin, *Sovetski J. Khimicheskaya Phizika* **1**, 2872 (1984), in Russian.
45. N. E. Ermolin, *Combust. Explos. Shock Waves* **31**, 58 (1995).
46. M. Tanaka and M. W. Beckstead, AIAA paper (1996) 96-2888.
47. M. W. Beckstead, J. E. Davidson and Q. Jing, in *Challenges in Propellants and Combustion/100 Years after Nobel*, ed. K. K. Kuo (Begell House Inc., New York-Wallingford, 1997).
48. H. K. Narahari, H. S. Mukunda and V. K. Jain, in *20th Symp. (Int.) on Combustion* (The Combustion Institute, Pittsburgh, PA, 1984), p. 2073.
49. N. Ilincic, M. A. Tanoff, M. D. Smooke, R. A. Yetter, T. P. Parr and D. M. Hanson-Parr, in *34th JANNAF Combustion Meeting*, Vol. II, CPIA Publication 662 (1997), p. 23.
50. R. S. Zhu and M. C. Lin, *Phys. Chem. Comm.* **25**, 1 (2001).
51. O. P. Korobeinichev, N. E. Ermolin, A. A. Chernov and I. D. Emel'yanov, *Fiz. Goreniya Vzryza* **28**, 53 (1992).
52. O. P. Korobeinichev, N. E. Ermolin, A. A. Chernov, I. D. Emel'yanov and T. V. Trofimycheva, *Fiz. Goreniya Vzryza* **26**, 46 (1990).
53. O. P. Korobeinichev, L. V. Kuibida, A. A. Paletsky, A. A. Chernov and N. E. Ermolin, *Prep. Pap. Am. Chem. Soc., Div. Fuel Chem.* **36**, 1582 (1991).
54. M. B. Jeppson, M. W. Beckstead and Q. Jing, AIAA paper (1998) 98-0447.
55. O. P. Korobeinichev, A. G. Tereschenko, V. M. Shvartsberg, G. A. Makhov, A. A. Chernov and A. E. Zabolotnyi, in *Flame Structure*, Vol. 1, ed. O. P. Korobeinichev (Nauka, Sibirskoe otdelenie, Novosibirsk, USSR, 1991), p. 262.
56. O. P. Korobeinichev, A. G. Tereschenko, V. M. Shvartsberg, G. A. Makhov, A. A. Chernov, A. E. Zabolotnyi and I. D. Emel'yanov, *Combust. Explos. Shock Waves* **26**, 173 (1990).
57. A. A. Chernov, V. M. Shvartsberg, N. E. Ermolin, O. P. Korobeinichev and V. M. Fomin, *Prep. Pap. Am. Chem. Soc., Div. Fuel Chem.* **39**, 188 (1994).
58. N. E. Ermolin, O. P. Korobeinichev, L. V. Kuibida and V. M. Fomin, *Combust. Explos. Shock Waves* **24**, 400 (1988).

59. M. Ben-Reuven and L. H. Caveny, *AIAA J.* **19**, 1276 (1981).
60. C. F. Melius, in *25th JANNAF Combustion Meeting*, Vol. II, CPIA Publication 498 (1988), p. 155.
61. C. F. Melius, in *Chemistry and Physics of Molecular Processes in Energetic Materials*, ed. S. Bulusu (Boston, Kluver, 1990), p. 51.
62. N. E. Ermolin and V. E. Zarko, *Fiz. Goreniya Vzryza* **37**, 3 (2001).
63. Y.-C. Lian and V. Yang, *J. Propul. Power* **11**, 729 (1995).
64. R. A. Yetter, F. L. Dryer, M. T. Allen and J. L. Gatto, *J. Propul. Power* **11**, 683 (1995).
65. J. J. Cor and J. J. Branch, *J. Propul. Power* **11**, 704 (1995).
66. K. Prasad, R. A. Yetter and M. D. Smooke, AIAA paper (1996) 96-0880.
67. B. E. Homan, M. S. Miller and J. A Vanderhoff, *Combust. Flame* **120**, 301 (2000).
68. T. Niioka, T. Mitani, H. Miyajima, N. Saito, T. Sohue, K. Ninomiyya and L. Aoki, *The Fundamental Study of HMX Composite Propellant and its Practical Application*, National Aerospace Laboratory Report, TR-875 (1985).
69. A. Zenin, *J. Propul. Power* **11**, 752 (1995).
70. O. P. Korobeinichev, L. V. Kuibida and V. Jh. Madirbaev, *Combust. Explos. Shock Waves* **20**, 282 (1984).
71. A. Bizot and M. W. Beckstead, in *Flame Structure*, Vol. 1, ed. O. P. Korobeinichev (Nauka, Novosibirsk, 1991), p. 230.
72. D. Hanson-Parr and T. Parr, in *25th Symp. (Int.) on Combustion* (The Combustion Institute, Pittsburg, PA, 1994), p. 1635.
73. C. J. Tang, Y. J. Lee, G. Kudva and T. A. Litzinger, *Combust. Flame* **117**, 170 (1999).
74. T. P. Parr and D. M. Hanson-Parr, in *35th JANNAF Combustion Meeting*, CPIA Publication 685 (1988), p. 87.
75. J. E. Davidson and M. W. Beckstead, in *26th Symp. (Int.) on Combustion* (The Combustion Institute, Pittsburg, PA, 1996), p. 1989.
76. Z. Pak, AIAA paper (1993) 93-1755.
77. B. L. Fetherolf and T. A. Litzinger, *Combust. Flame* **114**, 515 (1998).
78. A. A. Zenin, V. M. Puchkov and S. V. Finjakov, AIAA paper (1998) 99-0595.
79. V. A. Strunin, A. P. D'Yakov and G. B. Manelis, *Combust. Flame* **117**, 429 (1999).
80. O. P. Korobeinichev, A. A. Paletsky, A. G. Tereschenko and T. A. Bolshova, in *Combustion of Energetic Materials*, ed. K. K. Kuo (Begell House Inc., New York, Wallingford, 2001), p. 486.
81. O. P. Korobeinichev, A. A. Paletsky, A. G. Tereschenko, E. N. Volkov, J. M. Lyon, J. G. Carver and R. L. Stanley, in *32nd Int. Ann. Conf. ICT*, Karlsruhe, Germany, 3–6 July, 2001, paper 123-1.
82. O. P. Korobeinichev, T. A. Bolshova and A. A. Paletsky, *Combust. Flame* **126**, 1516 (2001).
83. A. E. Fogelzang, V. P. Sinditski, V. Y. Egorshev, A. I. Levshenkov, V. V. Serushkin and V. I. Kolesov, in *28th Int. Ann. Conf. ICT*, Karlsruhe, Germany, 1997, paper 99-1.

84. O. P. Korobeinichev, L. V. Kuibida, A. A. Paletsky and A. G. Shmakov, in *Proc. 21st Int. Symp. on Space Technology and Sciences*, Vol. 1 (Society for Aeronautical and Space Sciences, Tokyo, 1998), p. 87.
85. A. G. Shmakov, O. P. Korobeinichev and T. A. Bolshova, *Combust. Explos. Shock Waves* **38**, 284 (2002).
86. J. Park, D. Chakraborty and M. C. Lin, in *27th Symp. (Int.) on Combustion* (The Combustion Institute, Pittsburgh, PA, 1998), p. 2351.
87. A. M. Mebel, M. C. Lin, K. Morokuma and C. F. Melius, *J. Phys. Chem.* **99**, 6842 (1995).
88. R. J. Kee, J. F. Grcar, M. D. Smooke and J. A. Miller, *Fortran Program for Modeling Steady Laminar One-Dimensional Premixed Flames*, Sandia Rept. SAND85-8240, Livermore, CA, 1989.
89. O. P. Korobeinichev and A. A. Paletsky, *Combust. Flame* **126**, 151 (2001).
90. L. V. Kuibida, O. P. Korobeinichev, A. G. Shmakov, E. N. Volkov and A. A. Paletsky, *Combust. Flame* **126**, 1655 (2001).
91. O. P. Korobeinichev, A. A. Paletsky, A. G. Tereschenko and E. N. Volkov, *J. Propul. Power* **19**, 203 (2003).
92. O. P. Korobeinichev, A. A. Paletsky, A. G. Tereschenko and E. N. Volkov, in *Proc. Combustion Institute*, Vol. 29 (2002), p. 2955.
93. A. A. Zenin, *Fiz. Goreniya Vzryza* **2**, 67 (1966), in Russian.

CHAPTER 4

OPTICAL SPECTROSCOPIC MEASUREMENTS OF ENERGETIC MATERIAL FLAME STRUCTURE

Tim Parr* and Donna Hanson-Parr†

Naval Air Warfare Center, Weapons Division
Code 4T4320D
China Lake, CA 93555-6106, USA
**Timothy.Parr@navy.mil*
†*Donna.Hanson-Parr@navy.mil*

Contents